RADIO SCIENCE Journal of Research NBS/USNC–URSI
Vol. 68D, No. 6, June 1964

ELF and VLF Waves Below an Inhomogeneous Anisotropic Ionosphere

Janis Galejs

Contribution From Applied Research Laboratory, Sylvania Electronic Systems, a Division of Sylvania Electric Products Inc., 40 Sylvan Road, Waltham, Mass., 02154

(Received December 17, 1963)

The differential equations developed by Galejs and Row in the analysis of ELF wave propagation for frequencies between 60 to 3000 c/s are modified to permit computations below the frequency of ion gyrofrequency. Near 8 c/s west-east propagation exhibits a minimum attenuation of 0.022 db/1000 km, while the east-west direction has a local maximum of 0.165 db/1000 km. The calculations in the frequency range between 20 and 3000 c/s are made with neglected ion effects, and the propagation is characterized by a monotonic decrease of phase velocity down to the lowest frequency.

The method used for calculating the surface impedance with an arbitrary profile of the ionospheric tensor conductivity and for strictly east-west, west-east, or south-north directions of propagation applies also to the VLF range. The VLF propagation characteristics are determined using the modal equation for a spherical earth-to-ionosphere geometry. Computations based on a simple exponential approximation to the ionospheric conductivity profile differ only slightly from computations made using more exact ionosphere parameters.

1. Introduction

The propagation of ELF waves below an inhomogeneous anisotropic ionosphere has been considered by Galejs and Row [1964]. The propagation is either transverse (east-west and west-east propagation) or longitudinal (south-north and north-south propagation) with respect to the horizontal magnetic field. For an arbitrary height variation of the tensor conductivity the surface impedance below the horizontally stratified noncurved ionosphere is computed by numerically integrating a differential equation. This work has considered the frequency range of 60 to 3000 c/s, where the lower frequency limit was determined by the accuracy of the numerical integration process.

In this note the differential equations of Galejs and Row [1964] will be modified in order to extend the validity of their numerical solutions to frequencies below the ion gyrofrequency (or into the frequency range of earth to ionosphere cavity resonance). The solutions of the differential equations also remain valid for higher frequencies and propagation characteristics of VLF waves can be determined using an appropriate modal equation. This would extend the work of Wait [1963c and 1963d] for isotropic and anisotropic ionosphere of exponential conductivity profiles to more general ionosphere models. Other work which has considered homogeneous ionosphere models in the VLF range [Wait, 1962, 1963a and b] may provide check cases for the present computations.

Section 2 of this note reviews the relevant ionosphere parameters and sections 3 and 4 summarize the surface impedance calculations, which follow closely Galejs and Row [1964]. The procedure used in calculating the propagation characteristics is outlined in section 5, and the numerical results are discussed in section 6.

2. The Ionosphere Model

Available data on electron and ion densities and collision frequencies have been summarized in figures 1 and 2 of Galejs and Row [1964]. These data can be used in the Appleton-Hartree formulas for the electrical conductivity of a lightly ionized species. Assuming a

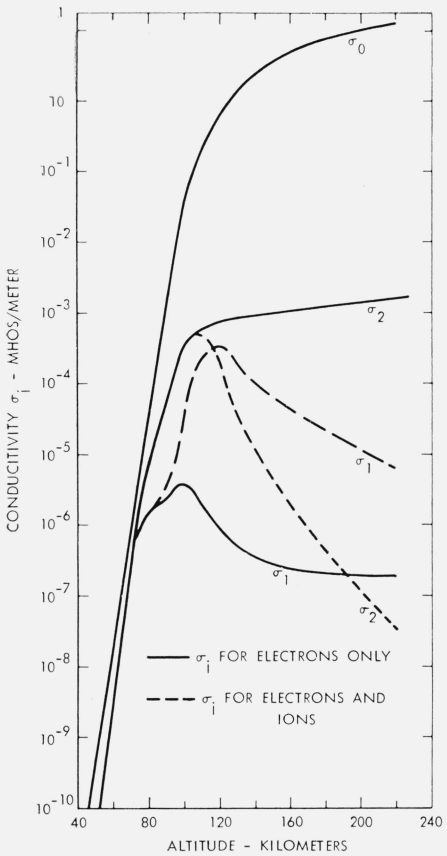

FIGURE 1. *Components of the daytime tensor conductivity* F=0.

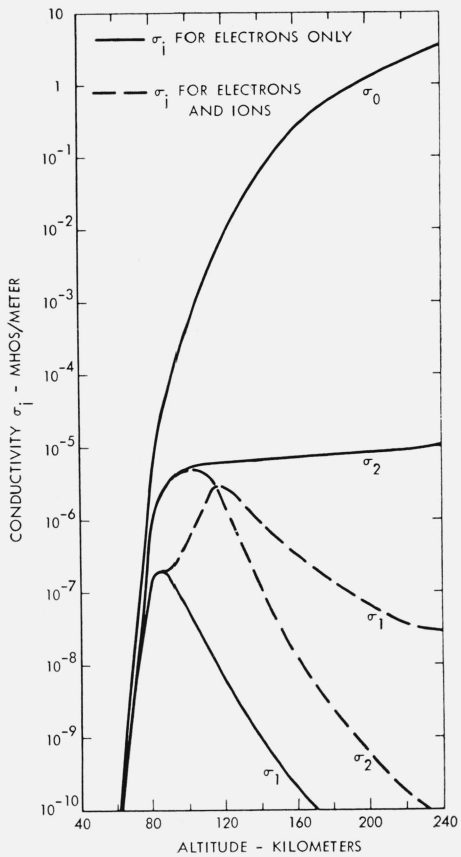

FIGURE 2. *Components of the nighttime tensor conductivity* F=0.

static magnetic field B_0 to act in the z direction the Cartesian form of the tensor conductivity for a harmonic field with time dependence exp $(-i\omega t)$ is,

$$[\sigma]=\begin{bmatrix}\sigma_1 & -\sigma_2 & 0\\ \sigma_2 & \sigma_1 & 0\\ 0 & 0 & \sigma_0\end{bmatrix} \tag{1}$$

where

$$\sigma_0=\epsilon_0\sum_k\frac{\omega_k^2}{\nu_k-i\omega} \tag{2}$$

$$\sigma_1=\epsilon_0\sum_k\frac{\omega_k^2(\nu_k-i\omega)}{(\nu_k-i\omega)^2+G_k^2} \tag{3}$$

$$\sigma_2=-\epsilon_0\sum_k\frac{\omega_k^2 G_k}{(\nu_k-i\omega)^2+G_k^2} \tag{4}$$

$$\omega_k=\left(\frac{n_k q_k^2}{\epsilon_0 m_k}\right)^{1/2} \tag{5}$$

is the plasma frequency of the kth charges species and n_k, q_k, m_k are the number density, charge and mass of the kth specie particle.

$$G_k=\frac{q_k B_0}{m_k} \tag{6}$$

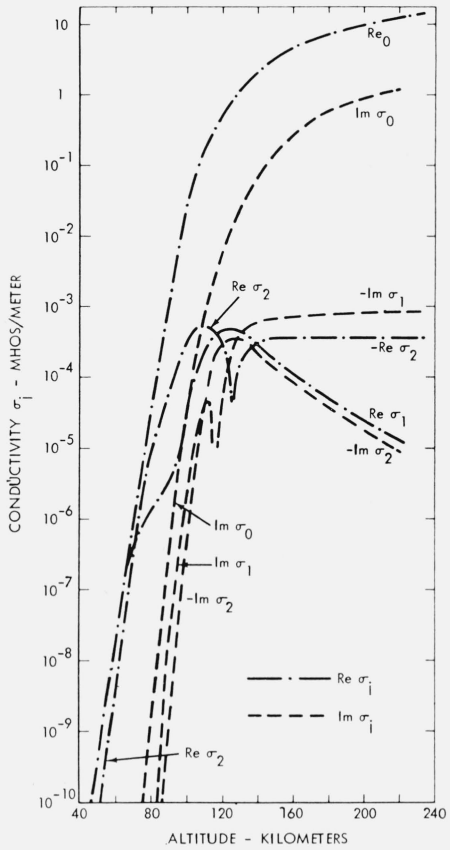

FIGURE 3. *Components of the daytime tensor conductivity* F=20 *c/s.*

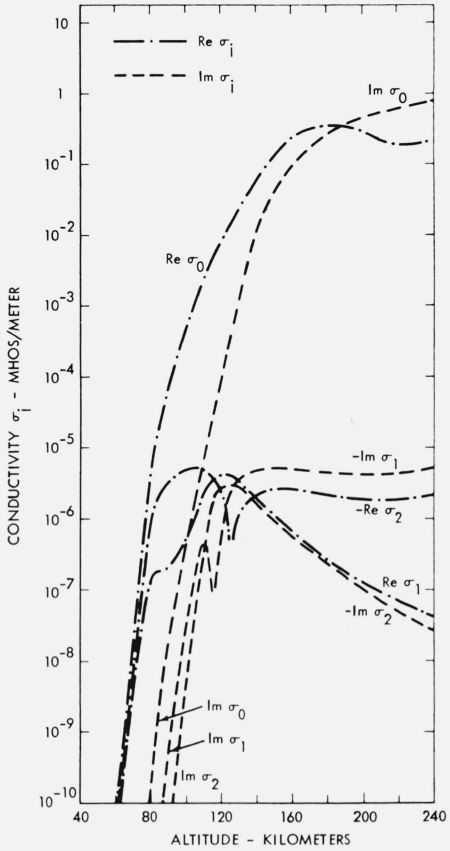

FIGURE 4. *Components of the nighttime tensor conductivity* F=20 *c/s.*

is the kth species gyrofrequency, ν_k is the effective collision frequency between kth species particle and all other constituents of the plasma. Considering electrons ($k=1$) in a static field of 0.5 oersted ($B_0=0.5\times10^{-4}$ MKS units), $\omega_1^2=3.185\ n_e\times10^3$, and $G_1=-1.04\times10^7$.

The components of the conductivity tensor have been plotted in figures 1 and 2 for $f=0$, in figures 3 and 4 for $f=20$ and in figures 5 and 6 for $f=15$ kc/s for both day and nighttime conditions. For $f=0$ the conductivity components are real, but the components become complex for $f\neq0$. For frequencies below the ion gyrofrequency the ionic plus electronic conductivity of $f=0$ is a good approximation to the real part of the complex conductivity ($f=20$ c/s). For frequencies above the ion gyrofrequency the electronic conductivity (the $k=1$ term of (2) to (4)) approximates the real part of the complex conductivity, particularly so for altitudes of less than 100 km. In the numerical calculations of propagation constants which make use of the electronic conductivity components for $f=0$, or of the electronic plus ionic conductivity for $f=15$ kc/s, the inequality $\sigma_2>>\sigma_1$ is satisfied for altitudes exceeding 100 km. This inequality does not apply to electronic plus ionic conductivity for $f=0$ or 20 c/s.

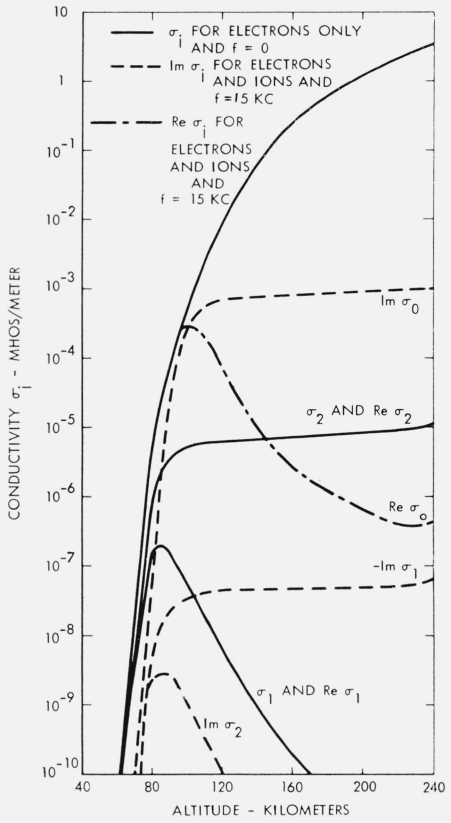

FIGURE 5. *Components of the daytime tensor conductivity* F=15 *kc/s.*

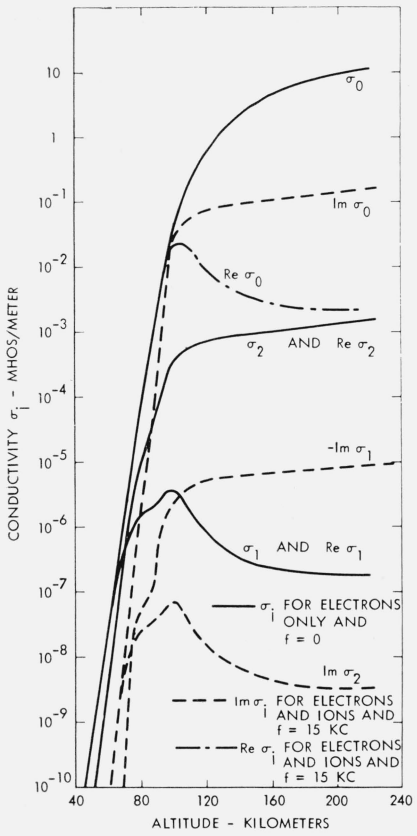

FIGURE 6. *Components of the nighttime tensor conductivity* F=15 *kc/s.*

3. Equatorial Propagation

For an assumed exp $(-i\omega t)$ time dependence of the fields the relative tensor permittivity is of the form

$$[\epsilon]=\begin{bmatrix}\epsilon_1 & -\epsilon_2 & 0\\ \epsilon_2 & \epsilon_1 & 0\\ 0 & 0 & \epsilon_3\end{bmatrix}=\begin{bmatrix}1+\dfrac{i\sigma_1}{\omega\epsilon_0} & -\dfrac{i\sigma_2}{\omega\epsilon_0} & 0\\ \dfrac{i\sigma_2}{\omega\epsilon_0} & 1+\dfrac{i\sigma_1}{\omega\epsilon_0} & 0\\ 0 & 0 & 1+\dfrac{i\sigma_0}{\omega\epsilon_0}\end{bmatrix} \tag{7}$$

if the static magnetic field is in the z direction. It is assumed that the field components exhibit no variation in the z direction and that $[\epsilon]$ is changing only in the y direction, which would be the south-north and vertical directions in terrestrial propagation problems. For east to west propagation along the magnetic equator the surface impedance below the anisotropic medium is given by Galejs and Row [1964] as

$$Z_s=-\frac{E_x}{H_z}$$

$$=[i\omega\epsilon_0(\epsilon_1^2+\epsilon_2^2)H_z]^{-1}\cdot\left[\epsilon_1\frac{\partial}{\partial y}H_z-\epsilon_2\frac{\partial}{\partial x}H_z\right]. \tag{8}$$

The sign of ϵ_2 is reversed for west to east propagation, which causes an obvious nonreciprocity. For propagation in the x direction the magnetic field component H_z will exhibit the x and y dependence of

$$H_z = \exp(ik_x x) Y(y). \tag{9}$$

$Y(y)$ is determined from a solution of the differential equation

$$\frac{d^2Y}{dy^2} + P(y)\frac{dY}{dy} + QY = 0 \tag{10}$$

where

$$P(y) = \frac{d}{dy}\log\left(\frac{\epsilon_1}{\epsilon_1^2+\epsilon_2^2}\right) \tag{11}$$

and

$$Q(y) = \frac{\epsilon_1^2+\epsilon_2^2}{\epsilon_1} k_0^2 - k_x^2 - ik_x \frac{\epsilon_2}{\epsilon_1}\frac{d}{dy}\log\left(\frac{\epsilon_2}{\epsilon_1^2+\epsilon_2^2}\right) \tag{12}$$

with $k_0 = \omega\sqrt{\epsilon_0\mu_0}$. The solution to this equation is formally given by

$$Y(y) = e^{-\frac{1}{2}\int P dy} f(y) = \left(\frac{\epsilon_1}{\epsilon_1^2+\epsilon_2^2}\right)^{-1/2} f(y) \tag{13}$$

where $f(y)$ satisfies the equation

$$\frac{d^2f}{dy^2} + K(y) = 0 \tag{14}$$

with

$$K(y) = Q - \frac{1}{2}\frac{dP}{dy} - \frac{1}{4}P^2. \tag{15}$$

The surface impedance (8) can be expressed in terms of $f(y)$ as

$$Z_s = \frac{1}{i\omega\epsilon_0}\left\{\left(\frac{\epsilon_1}{\epsilon_1^2+\epsilon_2^2}\right)\left[V(y) - \frac{1}{2}P(y)\right] - \frac{\epsilon_2}{\epsilon_1^2+\epsilon_2^2} ik_x\right\} \tag{16}$$

where

$$V(y) = \frac{1}{f}\frac{df}{dy}. \tag{17}$$

$V(y)$ satisfies the Riccati-type differential equation

$$\frac{dV}{dy} = -[V(y)^2 + K(y)]. \tag{18}$$

However, $V(y)$ becomes approximately equal to $\frac{1}{2}P(y)$ for the lower frequencies near the lower ionosphere boundary, and minor errors in the numerical integration cause significant inaccuracies in Z_s. This difficulty can be avoided by defining a new variable

$$U(y) = V(y) - \frac{1}{2}P(y). \tag{19}$$

Substitution of (19) in (18) shows that $U(y)$ satisfies the differential equation

$$\frac{dU}{dy} = -U^2(y) - P(y)U(y) - Q(y), \tag{20}$$

which can be integrated numerically if $U = U(y_u)$ is specified at a given altitude $y = y_u$. $U(y_u)$ may be determined from the surface impedance Z_s at the upper edge $y = y_u$ of the ionosphere model. Examination of the conductivity profiles of figures 1 and 2 indicates that $\sigma_2 >> \sigma_1$ at

$y>100$ km with ions neglected or for $\omega>G_{\text{ion}}$ with ions considered. Assuming an exponential variation of σ_2 for $y>y_u>100$ km and setting $\epsilon_1=$constant, $U(y_u)$ is computed as

$$U(y_u)=ik_0\frac{\epsilon_2}{\sqrt{\epsilon_1}}. \tag{21}$$

It may be also assumed that σ_1 and $\sigma_2=$constant for $y>y_u$. The corresponding value of $U(y_u)$ is

$$U(y_u)=ik_0\sqrt{\frac{\epsilon_1^2+\epsilon_2^2}{\epsilon_1^2}}, \tag{22}$$

which is applicable to any ratio of σ_2/σ_1. The above equations apply to east to west propagation. For west to east propagation ϵ_2 in (12), (15), and (16) should be multiplied by minus one.

4. Propagation Across the Magnetic Equator

Near the magnetic equator the static earth's magnetic field is in the south to north direction, which is the z-direction in the definition of the permittivity tensor (7). The tensor $[\epsilon]$ changes only in the vertical y-direction and the field components exhibit no variation in the x-direction (west to east direction). The differential equations of the various field components are generally coupled. However, in the lower ionosphere the coupling may be neglected [Galejs and Row, 1964] and the surface impedance for vertically polarized fields is simply

$$Z_s=\frac{E_z}{H_x}=\frac{1}{i\omega\epsilon_0\epsilon_3}\frac{1}{H_x}\frac{\partial}{\partial y}H_x. \tag{23}$$

H_x is of the form

$$H_x=\exp(ik_z z)Y(y). \tag{24}$$

$Y(y)$ is determined from the solution of the differential equation

$$\frac{\epsilon_1}{\epsilon_3}\frac{d^2Y}{dy^2}-\frac{\epsilon_1}{\epsilon_3^2}\frac{d\epsilon_3}{dy}\frac{dY}{dy}+(\epsilon_1k_0^2-qk_z^2)Y=0. \tag{25}$$

The parameter q of (25) characterizes the amount of coupling between TE and TM field components (or between E_x and H_x) at a given altitude y. There is negligible coupling with $q=1$ near the lower ionosphere boundary, but the amount of coupling is increased and the magnitude of q is decreased with increasing altitude. The simplest approximation of

$$q=\begin{cases}1 \text{ for } y<y_1\\ 0 \text{ for } y\geq y_1\end{cases} \tag{26}$$

implies negligible coupling between E_x and H_x for $y<y_1$, and strong coupling for $y\geq y_1$. This artificial boundary at $y=y_1$ will introduce an impedance discontinuity at a height where it appears to have little effect on fields below. In analogy with section 3, the surface impedance is given by

$$Z_s=\frac{1}{i\omega\epsilon_0}\frac{1}{\epsilon_3}\left[V(y)-\frac{1}{2}P(y)\right]=\frac{1}{i\omega\epsilon_0}\frac{1}{\epsilon_3}U(y) \tag{27}$$

where

$$P(y)=-\frac{d}{dy}(\log\epsilon_3). \tag{28}$$

$U(y)$ is determined from the solution (20) where $Q(y)$ is given by

$$Q(y)=\epsilon_3k_0^2-\frac{\epsilon_3}{\epsilon_1}qk_z^2. \tag{29}$$

The differential equation (20) is integrated downward from $y=y_u>y_1$. The starting value $U(y_u)$ is computed for an exponential height variation of ϵ_3 and for ϵ_1=constant. It follows that

$$U(y_u)=i\sqrt{k_0^2-qk_z^2/\epsilon_1}\sqrt{\epsilon_3}. \tag{30}$$

In view of (26) $U(y_u)$ of (30) is changed to

$$U(y_u)=ik_0\sqrt{\epsilon_3}. \tag{31}$$

5. Propagation Characteristics

5.1. ELF

For ELF waves the propagation constant ik_x of section 3 or ik_z of section 4 is given by ik_0S, where S is computed following Galejs [1961] from an iteration solution of

$$S_n=\sqrt{1+\frac{1}{k_0y n_i^e(S_{n-1})}\sqrt{1-\left[\frac{S_{n-1}}{n_i^e(S_{n-1})}\right]^2}} \tag{32}$$

where

$$(n_i^e)^2\approx\frac{\mu_0}{\epsilon_0 Z_s^2}\left[\frac{1}{2}+\sqrt{\frac{1}{4}-\frac{S^2Z_s^2\epsilon_0}{\mu_0}}\right]. \tag{33}$$

Z_s is computed at the assumed boundary height y of the ionospheric profile. Z_s of (8), (16), (23), or (27) depend also on S. The subscripts of S designate the successive iterations, and the calculations may be started with $S_0=1$ in the right-hand side of (32).

5.2. VLF

The propagation characteristics of the VLF waves are calculated starting out with (VII–27) of Wait [1962], which is rewritten for exp $(-i\omega t)$ time dependence as

$$\left[\frac{w_1'(t)-q_g w_1(t)}{w_2'(t)-q_g w_2(t)}\right]\left[\frac{w_2'(t-u)+q_i w_2(t-u)}{w_1'(t-u)+q_i w_1(t-u)}\right]=e^{i2\pi n} \tag{34}$$

where

$$-t=\left(\frac{k_0a}{2}\right)^{2/3}C^2, \tag{35}$$

$$u=\left(\frac{2}{k_0a}\right)^{1/3}k_0y, \tag{36}$$

$$q_j\simeq i\left(\frac{k_0a}{2}\right)^{1/3}\Delta_j, \tag{37}$$

$$\Delta_g\simeq\sqrt{\frac{i\omega\epsilon_0}{i\omega\epsilon_g-\sigma_g}}, \tag{38}$$

$$\Delta_i=\sqrt{\frac{\epsilon_0}{\mu_0}}Z_s, \tag{39}$$

$w_1(t)$ and $w_2(t)$ are the Airy functions, n is the mode number, a is the radius of the earth, and C is a root of the modal equation ($C^2=1-S^2$). The Airy functions may be represented by a power series or they can be related to Bessel or Hankel functions [Spies and Wait, 1961]. The Airy functions of arguments $(t-u)$ are expressed in terms of Hankel functions as in (VII–42) of Wait [1962], which are replaced by asymptotic expansions. This gives

$$\log(-R_i)+\log\frac{w_1'(t)-q_g w_1(t)}{w_2'(t)-q_g w_2(t)}+i\frac{2}{3}k_0a(C')^3-i\frac{\pi}{2}(4n-1)=0 \tag{40}$$

with

$$R_i=\frac{C'\left[1+\frac{7}{24}\frac{i}{k_0a(C')^3}\right]-\Delta_i\left[1-\frac{5}{24}\frac{i}{k_0a(C')^3}\right]}{C'\left[1-\frac{7}{24}\frac{i}{k_0a(C')^3}\right]+\Delta_i\left[1+\frac{5}{24}\frac{i}{k_0a(C')^3}\right]}. \tag{41}$$

$$C'=\sqrt{C^2+\frac{2y}{a}}. \tag{42}$$

Approximate solutions of (40) can be worked out on the assumptions $k_0a(C')^3>>1$, $(C'/\Delta_i)<1$, $C^2<<(2y/a)$ and $q_g<<1$. Approximating the term of (40) which involves Airy functions by its $C=0$ value, expanding $\log(-R_i)$ in powers of (C'/Δ_i) and introducing a further approximation

$$(C')^{2m+1}\approx\left(\frac{2y}{a}\right)^{\frac{2m+1}{2}}\left[1+\frac{2m+1}{2}\frac{C^2}{\frac{2y}{a}}\right] \tag{43}$$

gives

$$C^2\approx\frac{(12n-5)\frac{\pi}{6}-\frac{4}{3}k_0y\sqrt{\frac{2y}{a}}-2i\sum_{m=0}^{M}\frac{1}{2m+1}\left(\frac{1}{\Delta_i}\sqrt{\frac{2y}{a}}\right)^{2m+1}}{k_0a\sqrt{\frac{2y}{a}}+\frac{ia}{2y}\sum_{m=0}^{M}\left(\frac{1}{\Delta_i}\sqrt{\frac{2y}{a}}\right)^{2m+1}} \tag{44}$$

where M must be such that the approximation (43) is still valid. For $(C'/\Delta_i)<<1$ only the $m=0$ terms of (44) are significant and (44) can be seen to become equivalent to (IX–19) of Wait [1962].

More accurate solutions of (40) are obtained by Newton's method. A Taylor series expansion of a function $f(z)$ about its approximate zero $f(z_0)$ gives a corrected z estimate for its zero as

$$z=z_0-\frac{f(z_0)}{df/dz|_{z=z_0}}. \tag{45}$$

Iterations may be used to improve accuracy of this process. Letting $z=C^2$, the initial value z_0 is obtained from (44) by assuming a perfectly reflecting ionosphere of $\Delta\to\infty$ (or $R_i\to-1$). The function $f(z_0)$ and its derivative follow from (40) as

$$f(z_0)=\log\frac{(\Delta_i-\alpha)-(C'+\beta)}{(\Delta_i-\alpha)+(C'+\beta)}+\log\frac{w_1'(t)-q_gw_1(t)}{w_2'(t)-q_gw_2(t)}+i\frac{2}{3}k_0a(C')^3-\frac{i\pi}{2}(4n-1), \tag{46}$$

$$\left.\frac{df}{dz}\right|_{z=z_0}=-\frac{1}{C'}\frac{(\Delta_i+\alpha)-\frac{\beta}{C'}(3\Delta_i-5\alpha)}{(\Delta_i-\alpha)^2-(C'+\beta)^2}+ik_0aC'+\frac{2i\left(\frac{k_0a}{2}\right)^{2/3}(t-q_g^2)}{[w_1'(t)-q_gw_1(t)][w_2'(t)-q_gw_2(t)]}, \tag{47}$$

where

$$\alpha=\frac{7i}{24k_0a(C')^2} \tag{48}$$

$$\beta=\frac{5i\Delta_i}{24k_0a(C')^3}. \tag{49}$$

For $\alpha=\beta=0$ and $C'<<\Delta_i$ (46) to (49) are equivalent to (VII–37) to (VII–40) of Wait [1962].

The propagation constant ik_x of section 3 or ik_z of section 4 is given by ik_0S where

$$S=\sqrt{1-C^2}. \tag{50}$$

The surface impedances Z_s of (16) and (27) are computed for the assumed lower boundary y of the ionospheric profile. Z_s is also dependent on S. S of (50) is computed using iterations by setting $S=1$ in the initial Z_s expression and by updating the S value in Z_s following each S computation. For modes of low attenuation the process is rapidly convergent and only a few iterations are necessary.

The above computational procedure differs from the method used by Wait [1963c] where the modal equation, similar to (44), is considered at a height $(y+\delta)$ which is above the lower boundary y of the ionosphere. A surface impedance is computed in a planar geometry at y, and the reflection coefficient $R_i(y)$ is referred to the height $(y+\delta)$ as for free space in this planar increment δ [Wait and Walters, 1963]. The reflection coefficient $R_i(y+\delta)$ becomes

$$R_i(y+\delta)=R_i(y)\exp(-i2k_0C\delta). \tag{51}$$

This is equivalent to transforming $\Delta_i(y)=\Delta_i$ into $\Delta_i(y+\delta)$ by

$$\frac{1}{\Delta_i(y+\delta)}=\frac{1}{\Delta_i}+ik_0\delta. \tag{52}$$

Substituting (52), $M=0$ and assuming $\delta<<y$, (44) may be rearranged into

$$C^2=\frac{(12n-5)\frac{\pi}{6}-\frac{4}{3}k_0y\sqrt{\frac{2y}{a}}-\frac{2i}{\Delta_i}\sqrt{\frac{2y}{a}}\left(1+\frac{\delta}{2y}\right)}{k_0a\sqrt{\frac{2y}{a}}+\frac{i}{\Delta_i}\sqrt{\frac{a}{2y}}\left(1-\frac{\delta}{2y}\right)} \tag{53}$$

which will differ from C^2 for $\delta\neq 0$, particularly if δ is a sizable fraction of y. The method which computes the surface impedance at y, but considers the modal equation at $y+\delta$ [Wait, 1963c], will therefore differ from computations which consider the modal equation also at y.[1] The latter approach is strictly correct only if the surface impedance is computed in a spherical geometry, or if the planar surface impedance is a good approximation to the spherical one. Impedance transformations similar to (52) but suitable for a spherical geometry are discussed in the appendix. The impedance error due to planar calculations can be decreased by selecting δ to be different from zero, although no such calculations are reported in this paper.

6. Discussion

The roots of the modal equation and the ELF attenuation rates have been calculated for the ionospheric conductivity profiles of figure 1 to 4. The ionospheric profile with considered ions for $f=20$ c/s applies to propagation below the ion gyrofrequency and was used for calculating the curves of figures 7 and 8. The plot in figure 7 shows a minimum of daytime Im S for east-west propagation around 8 c/s. Im S for west-east direction has a maximum at this frequency. The corresponding attenuation rate figures are $\alpha_{ew}=0.165$ db/1000 km, and $\alpha_{we}=0.022$ db/1000 km. The field enhancement near the first resonant frequency of the earth-to-ionosphere cavity appears, therefore, due more to west-east than to east-west directions of propagation. The roots of the modal equations and the attenuation rates have been also calculated for electronic conductivity ($f=0$) in the frequency range of 20 to 2000 c/s and are shown in figures 9 to 11. It was already pointed out that this appears to be a satisfactory approximation to the computed conductivity profiles for frequencies above the ion gyrofrequency. In distinction from earlier work [Galejs and Row, 1964], the Re S is now mono-

[1] Such comments do not apply to planar geometry (e.g., eq VI-4.1 of Wait [1962]) where a change of the boundary height of the modal equation and a simultaneous transformation of R_i as in (51) do not affect the solution. However, the planar mode equation is not considered accurate in the VLF range.

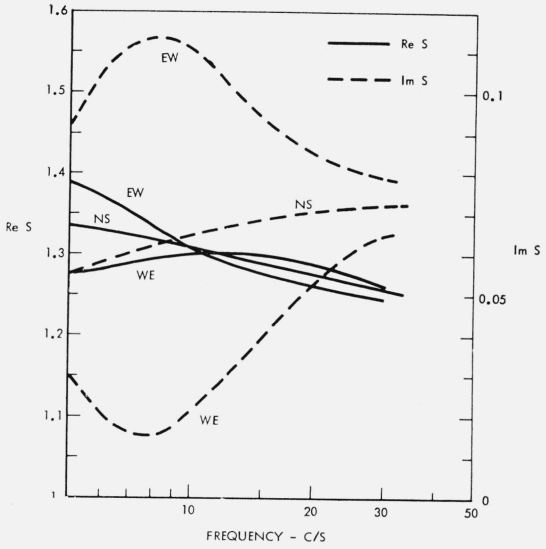

FIGURE 7. *Roots of the modal equation.*
Daytime conductivity with ions considered (fig. 3).

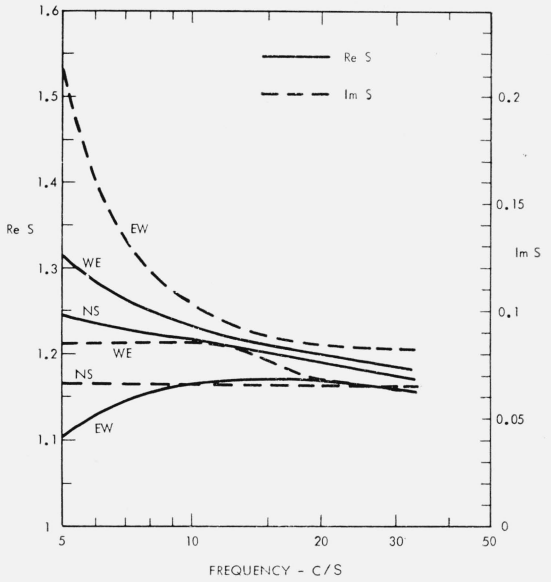

FIGURE 8. *Roots of the modal equation.*
Nighttime conductivity with ions considered (fig. 4).

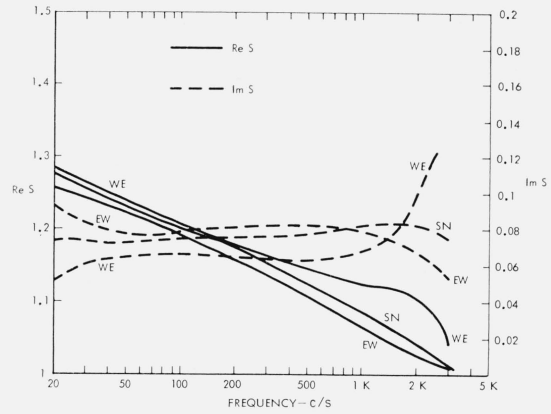

FIGURE 9. *Roots of the modal equation.*
Electronic daytime conductivity for f=0 (fig. 1).

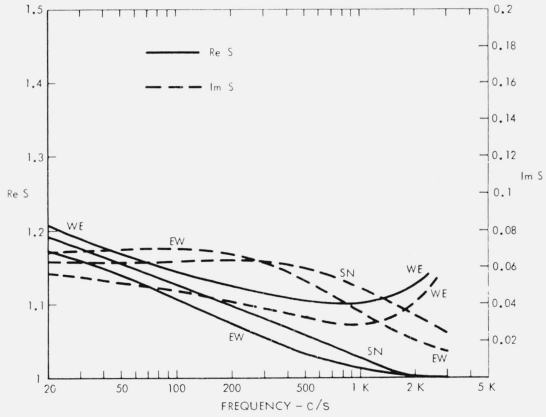

FIGURE 10. *Roots of the modal equation.*
Electronic nighttime conductivity for f=0 (fig. 2).

tonically increasing or the phase velocity monotonically decreasing down to the lowest frequencies of the plot. The high-frequency behavior of these curves is about the same as in the computations by Galejs and Row [1964].

The calculations in the VLF range were first made for a sharply bounded homogeneous ionosphere to obtain a check with published results. The ionospheric conductivity is represented by the tensor (7). The computed curves are similar to those of Wait [1962], which were obtained by a different method. East-west direction exhibits the higher attenuation. The differences between the Re S figures are almost indistinguishable, although Re S_{ew} exhibits the higher values. The curves for an isotropic ionosphere are intermediate between those of east-west and west-east directions.

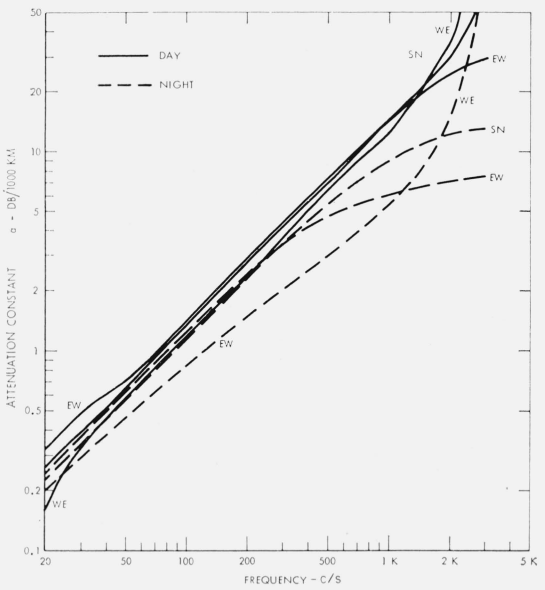

FIGURE 11. *Attenuation constants. Electronic conductivity for* f=0 *(figs. 1 and 2).*

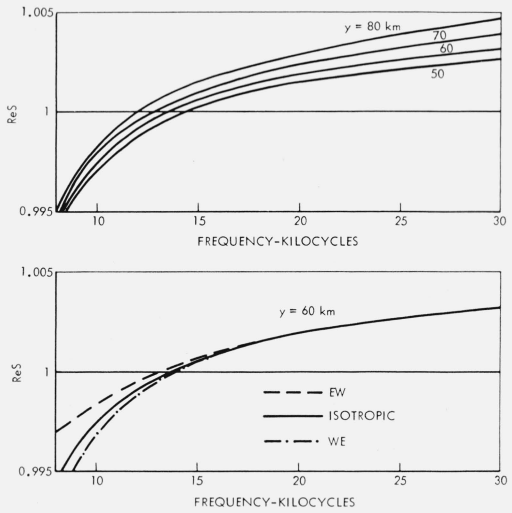

FIGURE 12. Re S *for exponential ionosphere model.* It is assumed that free space exists below the indicated values of y. Similar remarks apply to figures 13 and 14.

The height of the lower ionosphere boundary which was used for surface impedance calculations is designated by y-const. in the figures.

The exponential ionosphere is assumed to have a conductivity profile of

$$\sigma_j = 10^{-6} \exp [0.291(y-74)] \tag{54}$$

where $j=1$ or 2 in the definition of the permittivity tensor (7) and y is in kilometers. The effects of frequency changes are shown in figures 12 and 13. Increasing the height of the lower ionosphere boundaries increases Re S or decreases the phase velocity ($v_p/c=1/\text{Re } S$) similarly as for the sharply bounded ionosphere. The attenuation rates show a significant change with different assumed heights of the lower ionosphere boundaries for the same ionospheric profile (54). These attenuation rates, obtained from the solution of (45) to (48) are compared in figure 14 with the approximate solution (44). There is a qualitative agreement, although differences of approximately 0.5 db may be noted.

The effects of profile shifts are illustrated in figures 15 and 16. An upward shift of the profile ($\delta>0$) increases Re S and decreases attenuation for a constant boundary height. The same conclusion applies in most cases to simultaneous profile and boundary shifts (e.g., $\delta=0$ and $+5$ curves are compared for boundaries at y and $y+5$ respectively). However, increasing the boundary height of a profile increases the attenuation rates significantly for y approaching 80 km.

These characteristics of attenuation rates apply to east-west, west-east propagation as well as to the isotropic ionosphere, and will be discussed with the aid of a surface impedance curve for the isotropic model shown in figure 17. The numerically calculated surface impedance can be checked against a closed form solution [Wait 1962, Galejs 1961] which is strictly valid for large magnitude of the local refractive index ($|n|=|1+i\sigma/\omega\epsilon_0|^{1/2}>>1$). The closed form solution agrees with numerical calculations for $y>$ 80 km, where the earlier nonequality is satisfied. For $y<60$ km the computer calculation and the free space approximation (52) both give about the same y dependence of Δ_i. The normalized surface impedance $|\Delta_i|$ is decreased in the height interval of 75 to 80 km where Re $\Delta_i \approx |\text{Im } \Delta_i|$. A decreasing Re Δ_i gives an increase of ($-$Im C^2) and hence of (Im S) or α following (44) which accounts for the α increase shown in figure 16. There is a minimum of α near $y=70$ km where Re Δ_i is maximum in figure 17. This reasoning does not apply to $y<60$ where Re $\Delta_i<$Im Δ_i, and where small Re Δ_i does not imply a large Im S or α.

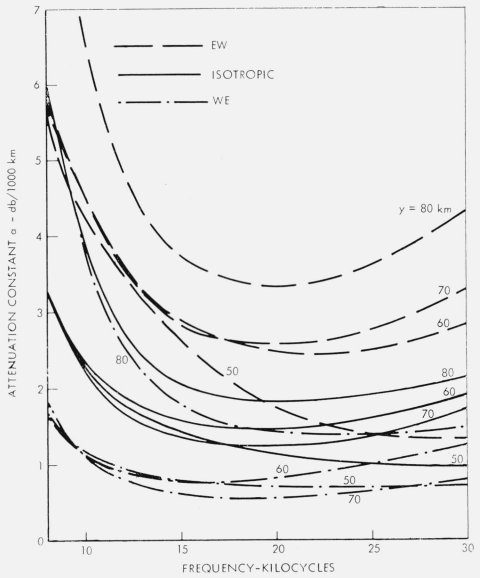

FIGURE 13. *Attenuation rates for exponential ionosphere model.*

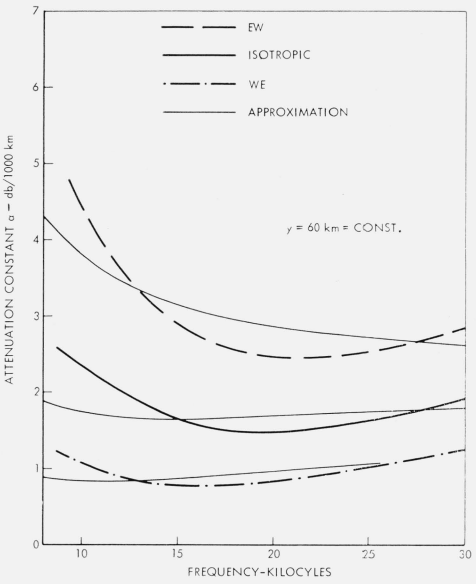

FIGURE 14. *Attenuation rates for exponential ionosphere model: comparison of approximations with more exact solutions.*

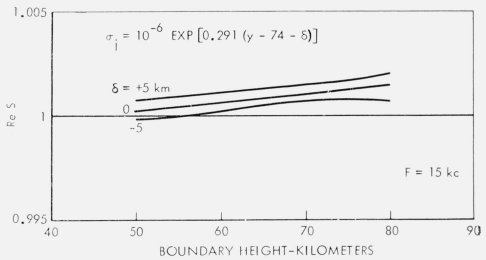

FIGURE 15. Re *S for shifted exponential profiles.*
Free space conditions are assumed below the boundary height.

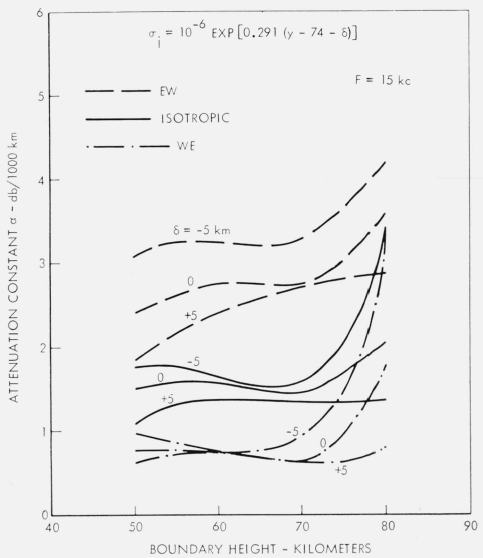

FIGURE 16. *Attenuation rates for shifted exponential profiles.*
Free space conditions are assumed below the boundary height.

Further calculations have been made for the daytime ionosphere conductivity profile of figure 5. The general behavior of the propagation parameters in figures 18 and 19 is similar to that shown in figures 12 and 13 for the simple exponential profile. A comparison with the approximate solution (44) is shown in figure 20, and comparisons with measurements [Watt and Croghan, 1963] are indicated in figure 21. There is a qualitative agreement although calculations give a nearly 1 db lower attenuation rate for north-south and west-south directions of propagation.

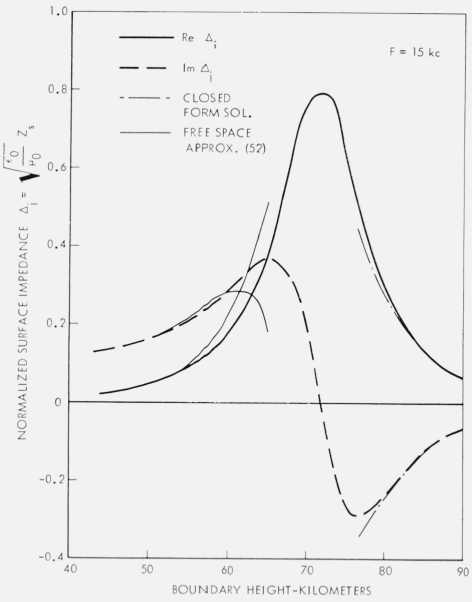

FIGURE 17. *Surface impedance for the isotropic exponential ionosphere model.*

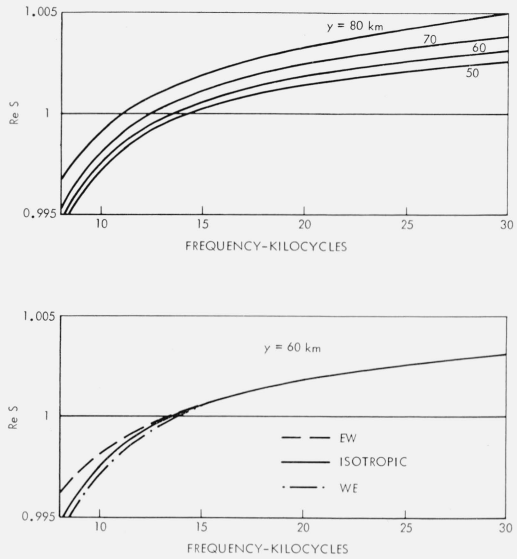

FIGURE 18. Re S *for daytime ionosphere; electronic plus ionic conductivity (fig. 5).*

It is assumed that free space exists below the indicated values of y. Similar remarks apply to figures 19, 20, and 21.

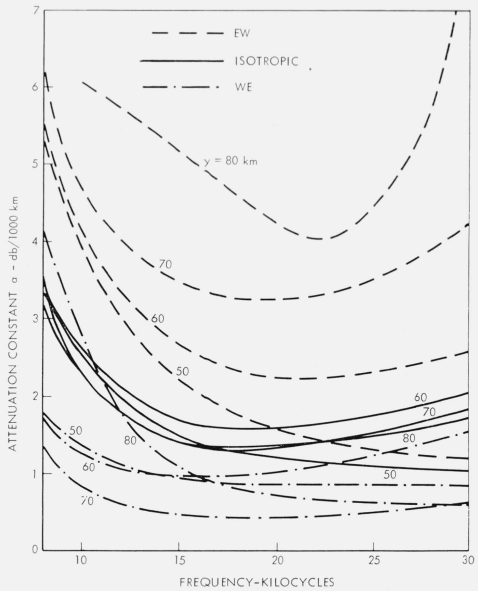

FIGURE 19. *Daytime attenuation rates; electronic plus ionic conductivity (fig. 5).*

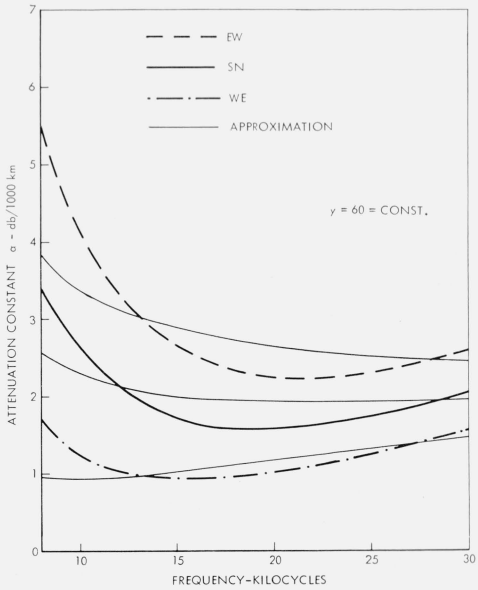

FIGURE 20. *Daytime attenuation rates; electronic plus ionic conductivity (fig. 5).*

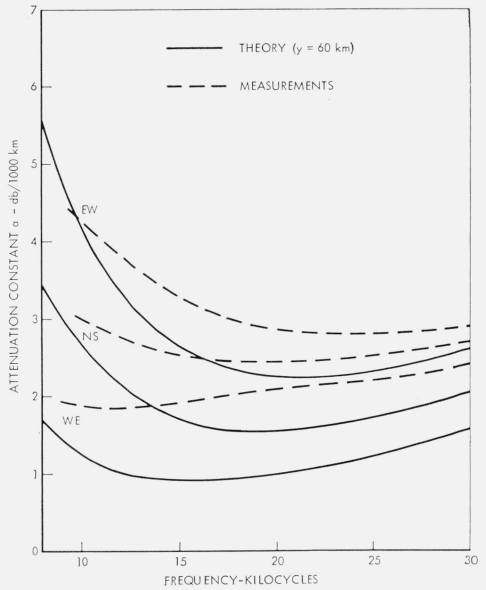

FIGURE 21. *Measured and calculated daytime attenuation rates.*

Calculations based on nighttime ionosphere profiles of figures 2 or 6 are less successful. Isotropic propagation results in α approximately 2 db/1000 km, the west-east and east-west directions exhibit $\alpha<0.5$ and $\alpha>3$ db/1000 km respectively. It is particularly difficult to justify the low α figure for the west-east direction of propagation and these numerical results are not shown in detail.

This work on the VLF propagation represents an initial attempt to consider a numerical surface impedance calculation in conjunction with the modal equations for spherical earth. The simple exponential conductivity profile gives about the same propagation constants as more elaborate ionosphere models, but the calculations are in both cases critically dependent on the assumed lower boundary height of the ionosphere model. A possible cause for this is the probable incompatibility between planar surface impedance calculations and the particular modal equation for spherical geometry. However, some improvement may be expected by referring the calculated planar surface impedance to a height near the equivalent reflection level of the ionosphere [Wait, 1963c]. It appears that further work is needed to clarify fully the effects of various boundary heights in the models of nonhomogeneous anisotropic ionosphere.

Appreciation is expressed to E. M. Larsen and J. Osborn for computational assistance. This work was supported by the Office of Naval Research under Contract Nonr 3185(00).

7. Appendix

Surface Impedance Transformation in a Spherical Geometry

The surface impedance computed at the bottom of the ionosphere y may be referred to a higher altitude $(y+\delta)$ if this does not alter the solutions of the modal equation. Such surface impedance transformations will be discussed in this appendix for the modal equations of section 4.2.

The modal equation (40) with R_i as in (41), but with neglected terms proportional to $(C')^{-3}$ has constant solutions if

$$\frac{\Delta_i - C'}{\Delta_i + C'} \exp\left[\frac{2ik_0a}{3}(C')^3\right] = \text{const.} \tag{55}$$

This is equivalent to transforming $\Delta_i(y) = \Delta_i$ to $\Delta_i(y+\delta)$ by

$$\frac{1}{\Delta_i(y+\delta)} = \frac{\frac{1}{\Delta_i} + \frac{i}{C'(y)} \tan\left[k_0\delta C'(y)\right]}{1 + \frac{iC'(y)}{\Delta_i} \tan\left[k_0\delta C'(y)\right]} \frac{C'(y)}{C'(y+\delta)} \tag{56}$$

with

$$\frac{C'(y)}{C'(y+\delta)} \approx 1 - \frac{\delta}{2y}\left(1 - \frac{C^2a}{y}\right). \tag{57}$$

For $k_0\delta C'(y) << 1$ (56) simplifies to

$$\frac{1}{\Delta_i(y+\delta)} = \left(\frac{1}{\Delta_i} + ik_0\delta\right)\left[1 - \frac{ik_0\delta}{\Delta_i}\frac{2y}{a}\left(1 + \frac{C^2a}{2y}\right) - \frac{\delta}{2y}\left(1 - \frac{C^2a}{2y}\right)\right]. \tag{58}$$

However, this form of impedance transformation does not provide a constant solution of the more approximate modal equation (44). The modal equation (44) with $M=0$ remains unaltered if

$$\frac{2C'}{\Delta} - \frac{2}{3} ik_0a(C')^3 = \text{const.} \tag{59}$$

This gives

$$\frac{1}{\Delta_i(y+\delta)} = \left(\frac{1}{\Delta_i} + ik_0\delta\right)\frac{C'(y)}{C'(y+\delta)} \tag{60}$$

where $C'(y)/C'(y+\delta)$ is given by (57). For $a \to \infty$, $C'(y) \to C'(y+\delta)$ following (42), and (60) reduces to (52). When applying (60) and (57) to (44), it is essential to keep the term proportional to C^2 in (57).

These surface impedance transformations should be used in connection with surface impedance calculations for a spherically stratified medium.

8. References

Galejs, J. (1961), ELF waves in the presence of exponential conductivity profiles, IRE Trans. Antennas Propagation **AP–9,** No. 6, 554–562.

Galejs, J., and R. V. Row (1964), Propagation of ELF waves below an inhomogeneous anisotropic ionosphere, IEEE Trans. Antennas Propagation **AP–12,** No. 1.

Spies, K. P., and J. R. Wait (1961), Mode calculations for VLF propagation in the earth-ionosphere waveguide, NBS Tech. Note No. 114, Appendix B.

Wait, J. R. (1962), Electromagnetic waves in stratified media (Pergamon Press, Oxford).

Wait, J. R. (1963a), The mode theory of VLF radio propagation for a spherical earth and a concentric anisotropic ionosphere, Can. J. Phys. **41,** No. 2, 299–315.

Wait, J. R. (1963b), Concerning solutions of the VLF mode problem for an anisotropic curved ionosphere, J. Res. NBS **67D** (Radio Prop.), No. 3, 297–302.

Wait, J. R. (1963c), Influence of the lower ionosphere on propagation of VLF radio waves to great distances, J. Res. NBS **67D** (Radio Prop.), No. 4, 375–381.

Wait, J. R. (1963d), Reflections of EM waves from stratified lossy plasma, VLF Symposium, Aug. 12, 13, and 14, Boulder, Colo.

Wait, J. R. and L. C. Walters, 1963, Reflection of VLF radio waves from an inhomogeneous ionosphere. Part I—Exponentially varying isotropic model, J. Res. NBS (Radio Propagation) Vol. 67D, No. 3, pp. 316–367.

Watt, A. D., and R. D. Croghan (1963), Comparison of observed VLF attenuation rates and excitation factors with theory, VLF Symposium, Aug. 12, 13, and 14, Boulder, Colo.

(Paper 68D6–367)